IEEE Robotics and Automation Letters (RA-L) paper, presented at ICRA 2024, Yokohama, Japan. Cite as RA-L paper.

Relative Localization Estimation for Multiple Robots via the Rotating Ultra-Wideband Tag

Jinxin Liu and Guoqiang Hu, *Senior Member, IEEE*

***Abstract*—Most distributed algorithms for robot coordination require relative location information, but how to obtain relative locations in a distributed manner is still a primary problem to address in multi-robot applications. In order to obtain the relative locations between robots, no matter whether they are in relative motion or stationary situation, we design a rotating ultra-wideband tag to provide the persistency of excitation condition and two estimation algorithms to estimate the relative locations in a distributed manner. Moreover, our approach relies only on on-board sensors and requires only one ultra-wideband tag per robot, eliminating the need for any ground anchors, thus allowing deployment in GNSS-denied environments without range restrictions. The proposed approach in this letter is also tested in simulations and experiments to verify the theoretical findings and effectiveness in practice.**

I. Introduction

MULTI-ROBOT systems, due to their physically distributed nature, can often perform tasks that a single robot is unable to accomplish. A growing number of researchers recognize the potential of multi-robot systems and have developed many distributed algorithms for multi-robot systems. The main obstacle in implementing distributed algorithms is acquiring the relative locations of the robots. Most localization methods can be divided into two categories, one relying on external anchors and the other relying only on on-board sensors.

The localization method relying on external anchor beacons can be categorized as the anchor-based method. The anchor-based methods often require running a centralized node to carry out the initial automatic calibration of the relative locations between anchors, and even some methods require the center node to provide real-time absolute location resolution services for each tag, which is contrary to the original design intent of most distributed algorithms, i.e., the relative location required by the distributed algorithm is provided by a centralized system. Global navigation satellite system (GNSS), ultra-wideband (UWB) with fixed anchors, and motion capture system are the most utilized anchor-based localization systems. In [1], GNSS is used to establish the location of each robot, but GNSS may become extremely inaccurate or even unavailable in GNSS-denied environments such as canyons, tunnels, or indoors. Motion capture systems [2] and UWB systems with fixed anchors [3]–[5] require pre-established anchors at the place where the localization service is needed. It limits the working area of robots to where the location service can be provided. Moreover, if the location of any one anchor is changed, the initial calibration needs to be done again.

The on-board localization method relies entirely on the robot's on-board sensors. The camera, one of the commonly used on-board sensors, is often used to obtain relative locations between robots [6]; however, on-board camera-based localization methods often suffer from occlusion, limited field of view, and short effective distance. Based on the inter-tag relative distance, some range-based on-board localization methods have been proposed. Particle filters are applied to process the data returned by all tags and their accompanying inertial measurement units [7], however, a centralized node is deployed to process the data, which consumes many computational resources. Four UWB tags are mounted on one robot to obtain the relative location in [8]–[10]. Both [11] and [12] obtain the relative location by three tags mounted on one robot. Moreover, the solution in [13] require only two tags to be installed on one robot. The above approaches require multiple tags to be mounted on one robot, which increases the cost of the localization system. Moreover, the effective distance for localization is directly proportional to the separation distance of the tags that are mounted on a robot. However, due to the restricted size of small robots, the effective distance is limited, rendering it inapplicable. Additionally, occlusion between tags may also result in non-line-of-sight propagation. In [14]–[16], only one UWB tag per robot needs to be installed, which means that only one distance measurement can be obtained between each robot pair. As summarized in [17], relying only on single-distance measurements with velocity information, the relative location is observable if the persistency of excitation condition is satisfied, which is why in [14]–[16] the robots must maintain relative motion in order to estimate the relative locations, whereas robots in multi-robot systems often need to maintain a fixed formation and have no relative motion to each other. To tackle the above issue, the main problem considered in this letter is how to estimate the relative locations between robots based on the single distance measurement no matter whether the robots are in relative motion or stationary.

The main contributions of this letter are as follows. First, a method of relative localization in the two-dimensional plane is proposed based on a rotating UWB tag. This method requires only one fixed or one rotating UWB tag per robot and achieves real-time relative localization no matter whether the robots are in relative motion or stationary, reducing the

This work was supported in part by the National Research Foundation, Singapore under its Medium Sized Center for Advanced Robotics Technology Innovation, and in part by Singapore Ministry of Education Academic Research Fund Tier 1 RG180/17(2017-T1-002-158). (Corresponding author: Guoqiang Hu.)

The authors are with the School of Electrical and Electronic Engineering, Nanyang Technological University, Singapore, Singapore 639798 jinxin001@e.ntu.edu.sg; gqhu@ntu.edu.sg.

IEEE Robotics and Automation Letters (RA-L) paper, presented at ICRA 2024, Yokohama, Japan. Cite as RA-L paper.

IEEE Robotics and Automation Letters (RA-L) paper, presented at ICRA 2024, Yokohama, Japan. Cite as RA-L paper.

costs of the whole system. Second, we demonstrate that the proposed algorithms converge exponentially in the ideal case. The effects of the height difference of the tags, the length of the rods, the rotation speed, the forgetting factor, and the noise level on the estimation are also analyzed. Third, the proposed approach's theoretical findings and effectiveness are verified through simulations and experiments.

II. Preliminaries and Problem Formulation

A. Kinematics of Robots

Consider a multi-robot system consisting of M clusters, where the clusters are indexed by $p \in \mathcal{M} = \{1, \cdots, M\}$. The $N_p + 1$ robots in cluster p can be denoted by the set $\bar{\mathcal{V}}_p = \{0_p, 1_p, \cdots, N_p\}$, with robot 0_p serving as the only leader robot in cluster p. The follower robots in cluster p can be represented by the set $\mathcal{V}_p = \bar{\mathcal{V}}_p \backslash \{0\}$. If two robots can exchange information between them, then these two robots are neighbors to each other. Within the cluster, each follower robot and its leader robot are neighbors to each other, and the leader robots of each cluster are neighbors to each other. For the sake of simplicity, the kinematics of the robot's base link center is assumed to represent the kinematics of the robot, and the kinematics of robot i in cluster p can be described by

$$\boldsymbol{x}_{i_p}[k] = \boldsymbol{x}_{i_p}[k-1] + \boldsymbol{v}_{i_p}[k-1]\Delta T, \quad k \geq 1, \tag{1}$$

where $\boldsymbol{x}_{i_p}[k] \in \mathbb{R}^2$ represents the absolute location of robot i_p in the world coordinate frame $\mathcal{F}_w$ at timestamp k, and robot i_p moves in two-dimensional plane. Similarly, $\boldsymbol{v}_{i_p}[k] \in \mathbb{R}^2$ represents the velocity of robot i_p in the frame $\mathcal{F}_w$ between timestamp $k-1$ and k. $\Delta T \in \mathbb{R}^+$ indicates the time interval between timestamps $k-1$ and k, which is also known as the sampling time. Robot $j_q \in \bar{\mathcal{V}}_q$ is one of robots in cluster $q \in \mathcal{M}$, and the relative location of robot i_p with respect to robot j_q in the frame $\mathcal{F}_w$ can be denoted by

$$\boldsymbol{x}_{i_p j_q}[k] = \boldsymbol{x}_{i_p}[k] - \boldsymbol{x}_{j_q}[k]. \tag{2}$$

In the frame $\mathcal{F}_w$, the relative velocity of robot i_p with respect to robot j_q is indicated by

$$\boldsymbol{v}_{i_p j_q}[k] = \boldsymbol{v}_{i_p}[k] - \boldsymbol{v}_{j_q}[k]. \tag{3}$$

B. The Rotating Ultra-Wideband Tag

To provide the persistency of excitation condition, we designed a rotating UWB tag device. The fixed-length rod is attached to and driven by the spindle of brushless motor, while the other end of the rod is mounted with a UWB tag, allowing the tag to circle around the center of the motor. The designed rotating UWB tag device only needs to be mounted on the leader robots, and the center of the spindle needs to coincide with the base link center. Each follower robot does not require installing the specially designed rotating UWB tag; instead, a fixed UWB tag installed at the base link center is sufficient. As a result, each robot is installed with only one UWB tag.

Without loss of generality, take the robots in the cluster p as an example. As shown in Fig. 1(a), in the frame $\mathcal{F}_w$, the absolute location of the UWB tag mounted on leader robot 0_p is represented by $\boldsymbol{x}_{u_{0_p}} \in \mathbb{R}^2$. $\mathcal{F}_{x_{0_p}}$ denotes the base link frame of leader robot 0_p. The rotation matrix $\boldsymbol{\mathcal{R}}^w_{x_{0_p}} \in \mathcal{SO}(2)$, which denotes the coordinate rotation matrix from frame $\mathcal{F}_{x_{0_p}}$ to frame $\mathcal{F}_w$, can be obtained by $\boldsymbol{\mathcal{R}}^w_{x_{0_p}} = \begin{bmatrix} \cos\phi_{0_p} & -\sin\phi_{0_p} \\ \sin\phi_{0_p} & \cos\phi_{0_p} \end{bmatrix}$, where ϕ_{0_p} can be obtained from the electronic compass. $l_p \in \mathbb{R}$ represents the length of the rod for the leader robot 0_p. $\theta_p \in \mathbb{R}$ is the angle between the rod and the x-axis of the frame $\mathcal{F}_{x_{0_p}}$, which can be measured by the encoder inside the motor. Thus, the absolute location of the leader robot 0_p and its mounted UWB tag have the following relationship

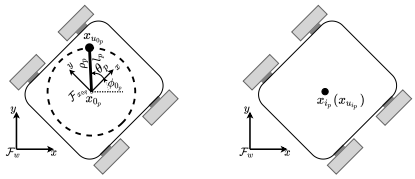

(a) Leader robot. (b) Follower robot.

Fig. 1. UWB tag installation for robots belonging to cluster p.

$$\boldsymbol{x}_{u_{0_p}}[k] = \boldsymbol{x}_{0_p}[k] + \boldsymbol{\rho}_p[k], \tag{4}$$

where $\boldsymbol{\rho}_p[k] = \boldsymbol{\mathcal{R}}^w_{x_{0_p}}[k]\,[l\cos\theta_p[k], l\sin\theta_p[k]]^\top \in \mathbb{R}^2$ denotes the offset of the rotating tag from the base link center in $\mathcal{F}_w$. According to equation (4), let $\boldsymbol{v}_{\rho_p}$ represents the relative velocity of the rotating tag with respect to the base link center, which could be obtained by $\boldsymbol{v}_{\rho_p}[k-1] = \frac{1}{\Delta T}(\boldsymbol{\rho}_p[k] - \boldsymbol{\rho}_p[k-1])$. As shown in Fig. 1(b), for the follower i_p, the tag is mounted in the center, i.e., $\boldsymbol{x}_{i_p} = \boldsymbol{x}_{u_{i_p}}$.

The UWB tag can measure the distance between itself and other tags, thus,

$$d_{i_p u_{0_p}}[k] = \|\boldsymbol{x}_{i_p}[k] - \boldsymbol{x}_{u_{0_p}}[k]\| = \|\boldsymbol{x}_{u_{i_p}}[k] - \boldsymbol{x}_{u_{0_p}}[k]\|, \tag{5}$$

$$d_{u_{0_p} u_{0_q}}[k] = \|\boldsymbol{x}_{u_{0_p}}[k] - \boldsymbol{x}_{u_{0_q}}[k]\|, \tag{6}$$

where $d_{i_p u_{0_p}} \in \mathbb{R}$ denotes the distance between the tags mounted on follower robot i_p and leader robot 0_p in cluster p, and $d_{u_{0_p} u_{0_q}} \in \mathbb{R}$ represents the distance between the rotating tags installed on the leaders of clusters p and q. It is worth noting that, due to the offsets $\boldsymbol{\rho}_p$, $d_{i_p u_{0_p}}$ is not equal to the distance between robots 0_p and i_p. Similarly, $d_{u_{0_p} u_{0_q}}$ is not equal to the distance between the leader of cluster p and the leader of cluster q.

C. Problem Formulation

Consider the multi-robot system, as shown in Fig. 2, leader robots of all clusters are equipped with the designed rotating UWB tag, and each follower is mounted with a fixed tag. This letter aims to develop algorithms for estimating the relative locations of robots based on the single-ranging measurement and the velocity of robots in a distributed manner. The relative localization problem can be divided into two categories, one is the estimation of relative locations between leaders and followers within a cluster, as shown in Fig. 2(a); and the other is the estimation of relative locations between leaders of different clusters, as shown in Fig. 2(b). Let $\hat{\boldsymbol{x}}_{i_p j_q}$ represent

IEEE Robotics and Automation Letters (RA-L) paper, presented at ICRA 2024, Yokohama, Japan. Cite as RA-L paper.

the estimation of the relative location $\boldsymbol{x}_{i_p j_q}$ given by proposed algorithms. Thus, the leader robot 0_p and its follower robot i_p can estimate the relative location between each other, i.e.,

$$\lim_{k\to\infty} \|\hat{\boldsymbol{x}}_{i_p 0_p}[k] - \boldsymbol{x}_{i_p 0_p}[k]\| = 0, \quad i_p \in \mathcal{V}_p, \quad p \in \mathcal{M}. \tag{7}$$

The leader robots can estimate the relative location between each other, i.e.,

$$\lim_{k\to\infty} \|\hat{\boldsymbol{x}}_{0_p 0_q}[k] - \boldsymbol{x}_{0_p 0_q}[k]\| = 0, \quad p, q \in \mathcal{M}. \tag{8}$$

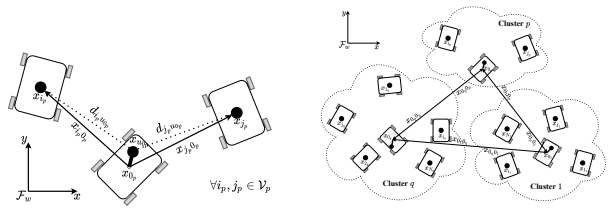

(a) Localization within cluster p. (b) Localization between clusters.

Fig. 2. Multi-robot relative localization based on a rotating UWB tag.

For the case where only one robot is equipped with a rotating tag and all other robots are equipped with fixed tags, i.e., all robots are in a cluster, the problem degenerates to problem (7). For the case where each robot is equipped with a rotating tag, i.e., each robot is the leader of its own cluster, the problem degenerates to problem (8). For the normal case with multiple rotating tags as well as fixed tags, the problem requires solving both problem (7) and (8). Moreover, the estimation of the relative locations of any two robots can be obtained by

$$\hat{\boldsymbol{x}}_{i_p j_q} = \hat{\boldsymbol{x}}_{i_p 0_p} + \hat{\boldsymbol{x}}_{0_p 0_q} + \hat{\boldsymbol{x}}_{0_q j_q}, \quad p, q \in \mathcal{M}. \tag{9}$$

It can be concluded that $\lim_{k\to\infty}\|\hat{\boldsymbol{x}}_{i_p j_q}[k] - \boldsymbol{x}_{i_p j_q}[k]\| = 0$ holds, if equations (7) and (8) hold. Since the estimation of relative locations between the leaders of different clusters can be broadcast by the cluster leader to the followers within the cluster, thus equation (9) can also be deployed in a distributed manner.

III. Main Results

A. Geometric Relationship

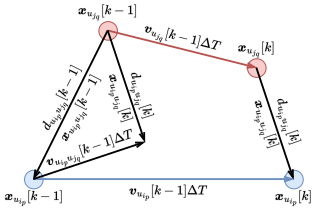

Fig. 3. Geometric relationships in relative motion.

Consider the motion of two tags u_{i_p} and u_{j_q} under two timestamps $k-1$ and k, which is shown in Fig. 3. $\boldsymbol{x}_{u_{i_p}}$ and $\boldsymbol{x}_{u_{j_q}}$ are the absolute locations of the two tags in the frame $\mathcal{F}_w$. $d_{u_{i_p} u_{j_q}}$ is thus the distance measured between the two tags. In addition, $\boldsymbol{x}_{u_{i_p} u_{j_q}}$ and $\boldsymbol{v}_{u_{i_p} u_{j_q}}$ represent relative location and relative velocity, respectively. The absolute locations of the two tags at two timestamps can be used as vertices to form a quadrilateral. Considering the relative motion from the perspective of tag i_p with respect to tag j_q, the quadrilateral degenerates to the triangle shown in Fig. 3. According to the law of cosines, the following holds,

$$\begin{aligned} &2\boldsymbol{\eta}^{\top}_{u_{i_p} u_{j_q}}[k-1]\boldsymbol{x}_{u_{i_p} u_{j_q}}[k-1] \\ =&(d^2_{u_{i_p} u_{j_q}}[k] - d^2_{u_{i_p} u_{j_q}}[k-1] - \|\boldsymbol{\eta}_{u_{i_p} u_{j_q}}[k-1]\|^2). \end{aligned} \tag{10}$$

where $\boldsymbol{\eta}_{u_{i_p} u_{j_q}}[k-1] = \boldsymbol{v}_{u_{i_p} u_{j_q}}[k-1]\Delta T$, which denotes the relative displacement between timestamps $k-1$ and k. It should be noted that even if the measurement triangle degenerates to a line segment, i.e., $\boldsymbol{v}_{u_{i_p} u_{j_q}}[k-1]$ is parallel to $\boldsymbol{x}_{u_{i_p} u_{j_q}}[k-1]$, the geometric relationship still holds.

B. Algorithm Design

Algorithm 1: Estimator for the relative location between leader 0_p and follower i_p in cluster p.

Input: Velocity of robots, i.e., $\boldsymbol{v}_{0_p}$ and $\boldsymbol{v}_{i_p}$, offset of the rotating tag, i.e., $\boldsymbol{\rho}_p$.

Result: Relative location estimation $\hat{\boldsymbol{x}}_{i_p 0_p}$.

Initialization: set forgetting factor $\gamma \in (0,1)$, initial estimation $\hat{\boldsymbol{x}}_{i_p 0_p}[0]$, initial weight matrix $\boldsymbol{P}[0]$;

while $k \geq 1$ **do**

  Calculate the last relative location estimation with respect to the rotating tag by $\hat{\boldsymbol{x}}_{u_{i_p} u_{0_p}}[k-1] = \hat{\boldsymbol{x}}_{i_p 0_p}[k-1] - \boldsymbol{\rho}_p[k-1]$;

  Calculate the relative velocity by $\boldsymbol{v}_{i_p 0_p}[k-1] = \boldsymbol{v}_{i_p}[k-1] - \boldsymbol{v}_{0_p}[k-1]$, $\boldsymbol{v}_{\rho_p}[k-1] = \frac{1}{\Delta T}(\boldsymbol{\rho}_p[k] - \boldsymbol{\rho}_p[k-1])$;

  Obtain the relative displacement by $\boldsymbol{\eta}_{u_{i_p} u_{0_p}}[k-1] = (\boldsymbol{v}_{i_p 0_p}[k-1] - \boldsymbol{v}_{\rho_p}[k-1])\Delta T$;

  Update the weight matrix by $\boldsymbol{P}[k] = \frac{1}{\gamma}(\boldsymbol{I} - \frac{\boldsymbol{P}[k-1]\boldsymbol{\eta}_{u_{i_p} u_{0_p}}[k-1]\boldsymbol{\eta}^{\top}_{u_{i_p} u_{0_p}}[k-1]}{\gamma + \boldsymbol{\eta}^{\top}_{u_{i_p} u_{0_p}}[k-1]\boldsymbol{P}[k-1]\boldsymbol{\eta}_{u_{i_p} u_{0_p}}[k-1]})\boldsymbol{P}[k-1]$;

  Update the error by $\epsilon[k] = \frac{1}{2}(d^2_{i_p u_{0_p}}[k] - d^2_{i_p u_{0_p}}[k-1] - \|\boldsymbol{\eta}_{u_{i_p} u_{0_p}}[k-1]\|^2) - \boldsymbol{\eta}^{\top}_{u_{i_p} u_{0_p}}[k-1]\hat{\boldsymbol{x}}_{u_{i_p} u_{0_p}}[k-1]$;

  Update the relative location estimation by $\hat{\boldsymbol{x}}_{i_p 0_p}[k] = \hat{\boldsymbol{x}}_{i_p 0_p}[k-1] + \boldsymbol{v}_{i_p 0_p}[k-1]\Delta T + \boldsymbol{P}[k]\boldsymbol{\eta}_{u_{i_p} u_{0_p}}[k-1]\epsilon[k]$;

end

Based on the geometric relationship in (10), Algorithm 1 is proposed to address the relative localization problem within each cluster defined in equation (7), while Algorithm 2 solves the relative localization problem between the clusters defined in equation (8).

In Algorithms 1 and 2, $\boldsymbol{P} \in \mathbb{R}^{2\times 2}$ denotes the weight matrix, and the initial weight matrix $\boldsymbol{P}[0]$ needs to be positive definite. The constant γ represents the forgetting factor. Typically, this factor is set to a value close to, but not equal to, one.

IEEE Robotics and Automation Letters (RA-L) paper, presented at ICRA 2024, Yokohama, Japan. Cite as RA-L paper.

To deploy Algorithm 1 in a distributed manner, each cluster leader needs to broadcast its velocity and the offset of the rotating tag to all the followers inside the cluster, while each follower in the cluster needs to send its velocity information to its leader. For the distributed deployment of Algorithm 2, the leaders of different clusters only need to exchange their velocity information and the offsets of their rotating tags with each other. Based on the estimations obtained from Algorithms

Algorithm 2: Estimator for the relative location between the leader robots of cluster p and q.

Input: Velocity of robots, i.e., $\boldsymbol{v}_{0_p}$ and $\boldsymbol{v}_{0_q}$, offsets of the rotating tags, i.e., $\boldsymbol{\rho}_p$ and $\boldsymbol{\rho}_q$.

Result: Relative location estimation $\hat{\boldsymbol{x}}_{0_p0_q}$.

Initialization: set forgetting factor $\gamma \in (0,1)$, initial estimation $\hat{\boldsymbol{x}}_{0_p0_q}[0]$, initial weight matrix $\boldsymbol{P}[0]$;

while $k \geq 1$ **do**

Calculate the last relative location estimation between the two rotating tags by $\hat{\boldsymbol{x}}_{u_{0_p}u_{0_q}}[k-1] = \hat{\boldsymbol{x}}_{0_p0_p}[k-1]+\boldsymbol{\rho}_p[k-1]-\boldsymbol{\rho}_q[k-1]$;

Calculate the relative velocity by $\boldsymbol{v}_{0_p0_q}[k-1] = \boldsymbol{v}_{0_p}[k-1] - \boldsymbol{v}_{0_q}[k-1]$, $\boldsymbol{v}_{\rho_p}[k-1] = \frac{1}{\Delta T}(\boldsymbol{\rho}_p[k] - \boldsymbol{\rho}_p[k-1])$, $\boldsymbol{v}_{\rho_q}[k-1] = \frac{1}{\Delta T}(\boldsymbol{\rho}_q[k] - \boldsymbol{\rho}_q[k-1])$;

Obtain the relative displacement by $\boldsymbol{\eta}_{u_{0_p}u_{0_q}}[k-1] = (\boldsymbol{v}_{0_p0_q}[k-1] + \boldsymbol{v}_{\rho_p}[k-1] - \boldsymbol{v}_{\rho_q}[k-1])\Delta T$;

Update the weight matrix by $\boldsymbol{P}[k] = \frac{1}{\gamma}(\boldsymbol{I} - \frac{\boldsymbol{P}[k-1]\boldsymbol{\eta}_{u_{0_p}u_{0_q}}[k-1]\boldsymbol{\eta}^\top_{u_{0_p}u_{0_q}}[k-1]}{\gamma+\boldsymbol{\eta}^\top_{u_{0_p}u_{0_q}}[k-1]\boldsymbol{P}[k-1]\boldsymbol{\eta}_{u_{0_p}u_{0_q}}[k-1]})\boldsymbol{P}[k-1]$;

Update the error by $\epsilon[k] = \frac{1}{2}(d^2_{u_{0_p}u_{0_q}}[k] - d^2_{u_{0_p}u_{0_q}}[k-1] - \|\boldsymbol{\eta}_{u_{0_p}u_{0_q}}[k-1]\|^2) - \boldsymbol{\eta}^\top_{u_{0_p}u_{0_q}}[k-1]\hat{\boldsymbol{x}}_{u_{0_p}u_{0_q}}[k-1]$;

Update the relative location estimation by $\hat{\boldsymbol{x}}_{0_p0_q}[k] = \hat{\boldsymbol{x}}_{0_p0_q}[k-1] + \boldsymbol{v}_{0_p0_q}[k-1]\Delta T + \boldsymbol{P}[k]\boldsymbol{\eta}_{u_{0_p}u_{0_q}}[k-1]\epsilon[k]$;

end

1, 2, and equation (9), any two follower robots i_p and j_q can also estimate the relative locations between them in a distributed manner. $\hat{\boldsymbol{x}}_{i_p0_p}$ and $\hat{\boldsymbol{x}}_{0_qj_q}$ can be obtained by robots i_p and j_q through Algorithm 1 and exchanged with each other. $\hat{\boldsymbol{x}}_{0_p0_q}$ can be obtained by their leaders through Algorithm 2 and broadcast to them.

C. Convergence Analysis

Let $\mathcal{K} = \{1, \cdots, k, \cdots\}$ denote the set of timestamps. To tackle the problems in the convergence analysis of Algorithm 1, we have the following assumptions.

Assumption 1. *Exist a constant s, and $\forall m \in \mathcal{K}$, $\exists s_1, s_2 \in \{m, \cdots, m+s-1\}$, $\boldsymbol{\eta}_{u_{i_p}u_{0_p}}[s_1] \not\parallel \boldsymbol{\eta}_{u_{i_p}u_{0_p}}[s_2]$ holds.*

Remark 1. *Assumption 1 implies that for every s timestamp, there exist at least two timestamps s_1 and s_2, such that the relative motion vectors between the rotating tag and the fixed tag are non-parallel. Usually, the rotation period of the rotating tag can be chosen as s. In every tag rotation cycle, there must exist two relative motion vectors are non-parallel.*

Remark 2. *In practice, Assumption 1 can be satisfied easily. For fixed robot formations, the relative velocity between robots, i.e., $v_{i_p0_p}$ is often zero vector. Due to the presence of the relative rotation of the rotating tag, i.e., $\boldsymbol{v}_{\rho_p}$ is time-varying, Assumption 1 is satisfied, which is the primary purpose of designing the rotating tag. It is worth noting that rotating tags do not have to rotate all the time, especially when there is a large relative motion between the cluster leader and its followers, but if the relative motion between robots is small, tag rotation is needed to provide larger excitation to suppress the noise. The most extreme case is where the relative motion between the robots during a rotation cycle is exactly the same as the rotating tag, i.e., $\boldsymbol{v}_{i_p0_p} = \boldsymbol{v}_{\rho_p}$, then $\boldsymbol{v}_{\rho_p}$ can be varied by changing the speed of rotation, the direction of rotation, and the length of the rod to make Assumption 1 hold.*

If Assumption 1 holds, then we have $\sum_{k=m}^{m+s-1} \boldsymbol{\eta}_{u_{i_p}u_{0_p}}[k-1]\boldsymbol{\eta}^\top_{u_{i_p}u_{0_p}}[k-1] \geq a_{i_p}\boldsymbol{I}$, $\forall m \in \mathcal{K}$, where $a_{i_p} = \min_{m\in\mathcal{K}} \lambda_{\min}(\sum_{k=m}^{m+s-1} \boldsymbol{\eta}_{u_{i_p}u_{0_p}}[k-1]\boldsymbol{\eta}^\top_{u_{i_p}u_{0_p}}[k-1]) > 0$.

Remark 3. *a_{i_p} describes the magnitude of the relative motion between the fixed tag i_p and the rotating tag 0_p during s time intervals. Thus for time-varying formations, the greater the magnitude of the relative motion between the follower and leader, the larger a_{i_p} tends to be. For fixed formations, the longer the rod or the faster it rotates, the larger a_{i_p} will be. However, it should be noted that when the rotation speed is too fast and the sampling time interval, i.e., ΔT, is too large, for example, one rotation period equals the time interval, it will make the rotating tag in the same position at each sampling point and thus reduce a_{i_p}.*

Proposition 1. *Assume Assumption 1 holds, for all $k \geq 0$, the weight matrix $\boldsymbol{P}^{-1}[k]$ is positive definite matrix. For all $k \geq s$, $\boldsymbol{P}^{-1}[k] \geq \frac{a_{i_p}(\gamma^{-1}-1)}{\gamma^{-s}-1}\boldsymbol{I}$.*

Proof. Base on the Algorithm 1, the update of the weight matrix $\boldsymbol{P}[k]$ follows the following equation

$$\boldsymbol{P}^{-1}[k] = \gamma\boldsymbol{P}^{-1}[k-1] + \boldsymbol{\eta}_{u_{i_p}u_{0_p}}[k-1]\boldsymbol{\eta}^\top_{u_{i_p}u_{0_p}}[k-1]. \quad (11)$$

$\boldsymbol{P}^{-1}[k]$ represents the weighted sum of the relative motions between the tags from the initial state, and the closer to timestamp k the greater its weight. Since $\boldsymbol{P}[0]$ is set as a positive definite matrix, and $\boldsymbol{P}^{-1}[k]$ is updated according to equation (11). It can be concluded that the weight matrix $\boldsymbol{P}^{-1}[k]$ is the positive definite matrix for all $k \geq 0$. If Assumption 1 holds, for any $m \in \mathcal{K}$, we have

$$\sum_{k=m}^{m+s-1} \boldsymbol{P}^{-1}[k] \geq \sum_{k=m}^{m+s-1} \boldsymbol{\eta}_{u_{i_p}u_{0_p}}[k-1]\boldsymbol{\eta}^\top_{u_{i_p}u_{0_p}}[k-1] \geq a_{i_p}\boldsymbol{I}, \quad (12)$$

Follow from the equation (11), it also can be concluded that

$$\boldsymbol{P}^{-1}[k] \geq \gamma\boldsymbol{P}^{-1}[k-1]. \quad (13)$$

IEEE Robotics and Automation Letters (RA-L) paper, presented at ICRA 2024, Yokohama, Japan. Cite as RA-L paper.

IEEE Robotics and Automation Letters (RA-L) paper, presented at ICRA 2024, Yokohama, Japan. Cite as RA-L paper.

Thus, following from inequality (13), we have

$$(1+\cdots+\frac{1}{\gamma^{s-1}})\boldsymbol{P}^{-1}[m+s-1] \geq \sum_{k=m}^{m+s-1} \boldsymbol{P}^{-1}[k]. \quad (14)$$

According to inequalities (12) and (14),

$$\boldsymbol{P}^{-1}[m+s-1] \geq \frac{a_{i_p}(\gamma^{-1}-1)}{\gamma^{-s}-1}\boldsymbol{I}. \quad (15)$$

For all $m \in \mathcal{K}$, the inequality (15) holds, thus $\boldsymbol{P}^{-1}[k] \geq \frac{a_{i_p}(\gamma^{-1}-1)}{\gamma^{-s}-1}\boldsymbol{I}, \quad \forall k \geq s.$ □

To simplify the Lyapunov function definition in the convergence analysis, let $\tilde{\boldsymbol{x}}_{i_pj_q} \in \mathbb{R}^2$ represent the error in the relative location estimation, which means $\tilde{\boldsymbol{x}}_{i_pj_q} = \boldsymbol{x}_{i_pj_q} - \hat{\boldsymbol{x}}_{i_pj_q}$. Thus, according to Algorithm 1 and equation (4), the estimation error between leader robot 0_p and follower robot i_p, i.e., $\tilde{\boldsymbol{x}}_{i_p0_p}$, satisfies

$$\tilde{\boldsymbol{x}}_{i_p0_p} = \boldsymbol{x}_{u_{i_p}u_{0_p}} + \boldsymbol{\rho}_p - \hat{\boldsymbol{x}}_{u_{i_p}u_{0_p}} - \boldsymbol{\rho}_p = \tilde{\boldsymbol{x}}_{u_{i_p}u_{0_p}}. \quad (16)$$

Following from the equations (10), (16), and the error update law in Algorithm 1, we have

$$\epsilon[k] = \boldsymbol{\eta}^{\top}_{u_{i_p}u_{0_p}}[k-1]\tilde{\boldsymbol{x}}_{i_p0_p}[k-1]. \quad (17)$$

According to the update law of relative location estimation in Algorithm 1 and the equation (17), the iterative formula for the estimation error can be obtained by the following equation,

$$\begin{aligned}
&\tilde{\boldsymbol{x}}_{i_p0_p}[k] \\
=&\tilde{\boldsymbol{x}}_{i_p0_p}[k-1] - \boldsymbol{P}[k]\boldsymbol{\eta}_{u_{i_p}u_{0_p}}[k-1]\epsilon[k] \\
=&(\boldsymbol{I} - \frac{\boldsymbol{P}[k-1]\boldsymbol{\eta}_{u_{i_p}u_{0_p}}[k-1]\boldsymbol{\eta}^{\top}_{u_{i_p}u_{0_p}}[k-1]}{\gamma+\boldsymbol{\eta}^{\top}_{u_{i_p}u_{0_p}}[k-1]\boldsymbol{P}[k-1]\boldsymbol{\eta}_{u_{i_p}u_{0_p}}[k-1]})\tilde{\boldsymbol{x}}_{i_p0_p}[k-1].
\end{aligned} \quad (18)$$

We now demonstrate the convergence analysis for the estimation error of Algorithm 1.

Theorem 1. *If Assumption 1 holds, robot updates its estimation by Algorithm 1, as timestamp k tends to infinity, the square of estimation error $\|\tilde{\boldsymbol{x}}_{i_p0_p}[k]\|^2$ will converge to zero exponentially at a rate of $\frac{(\gamma^{-s}-1)\lambda_{\max}(\boldsymbol{P}^{-1}[0])}{a_{i_p}(\gamma^{-1}-1)}\gamma^k$.*

Proof. Choose the following Lyapunov function

$$V[k] = \tilde{\boldsymbol{x}}^{\top}_{i_p0_p}[k]\boldsymbol{P}^{-1}[k]\tilde{\boldsymbol{x}}_{i_p0_p}[k] \in \mathbb{R}. \quad (19)$$

Then,

$$\begin{aligned}
&V[k] - V[k-1] \\
\leq&(\gamma-1)\tilde{\boldsymbol{x}}^{\top}_{i_p0_p}[k-1]\boldsymbol{P}^{-1}[k-1]\tilde{\boldsymbol{x}}_{i_p0_p}[k-1] \\
=&(\gamma-1)V[k-1].
\end{aligned} \quad (20)$$

Thus, it can be concluded that $V[k] \leq \gamma^k V[0]$. If Assumption 1 holds, according to Proposition 1, we have

$$\|\tilde{\boldsymbol{x}}_{i_p0_p}[k]\|^2 \leq \frac{(\gamma^{-s}-1)\lambda_{\max}(\boldsymbol{P}^{-1}[0])}{a_{i_p}(\gamma^{-1}-1)}\gamma^k\|\tilde{\boldsymbol{x}}_{i_p0_p}[0]\|^2. \quad (21)$$

As $k \to \infty$, $\gamma^k \to 0$, thus, it can be concluded that $\|\tilde{\boldsymbol{x}}_{i_p0_p}[k]\| \to 0$. □

Remark 4. *The estimation error is related to the initial weight matrix $\boldsymbol{P}[0]$, which can be set as a diagonal matrix with large diagonal elements, which helps the error to converge to an acceptable range quickly. Similarly, suppose the initial estimation $\hat{\boldsymbol{x}}_{i_p0_p}[0]$ is closer to the initial true value $\boldsymbol{x}_{i_p0_p}[0]$, the estimation error can also quickly converge to a reasonable range. Moreover, a smaller forgetting factor leads to a faster convergence rate. Furthermore, it is worth noting that a larger a_{i_p} also leads to a faster convergence rate, so it follows from Remark 3 that a greater relative motion between the robots and a longer rod length as well as a faster rotation rate of the rotating tag lead to a faster convergence rate.*

Theorem 1 is to address the problem formulated in equation (7). To tackle the problem formulated in equation (8), we have the following Theorem 2.

Assumption 2. *Exist a constant s, and $\forall m \in \mathcal{K}$, $\exists s_1, s_2 \in \{m, \cdots, m+s-1\}$, $\boldsymbol{\eta}_{u_{0_p}u_{0_q}}[s_1] \nparallel \boldsymbol{\eta}_{u_{0_p}u_{0_q}}[s_2]$ holds.*

Remark 5. *Assumption 2 implies that there exists two non-parallel relative motion vectors between the two rotating tags within every s time interval. Similar to Assumption 1, Assumption 2 can also be easily satisfied. Taking the example that the leaders of clusters p and q need to keep a time-invariant formation, that is, $\boldsymbol{v}_{0_p0_q} = \boldsymbol{0}_2$, $\boldsymbol{v}_{\rho_p} - \boldsymbol{v}_{\rho_q}$ can be made to be time-varying by setting the two rotating tags to have the same rotation speed but different initial phases, i.e., $\boldsymbol{\rho}_p[0] \neq \boldsymbol{\rho}_p[0]$ or different rotation speeds.*

Theorem 2. *If Assumption 2 holds, robot updates its estimation by Algorithm 2, as timestamp k tends to infinity, the square of estimation error $\|\tilde{\boldsymbol{x}}_{0_p0_q}[k]\|^2$ will converge to zero exponentially at a rate of $\frac{(\gamma^{-s}-1)\lambda_{\max}(\boldsymbol{P}^{-1}[0])}{b_{pq}(\gamma^{-1}-1)}\gamma^k$, and $b_{pq} = \min_{m\in\mathcal{K}}\lambda_{\min}(\sum_{k=m}^{m+s-1}\boldsymbol{\eta}_{u_{0_p}u_{0_q}}[k-1]\boldsymbol{\eta}^{\top}_{u_{0_p}u_{0_q}}[k-1])$.*

The proof of Theorem 2 is similar to that of Theorem 1, so it is omitted here.

Remark 6. *Similar to Remark 4, the rate of convergence for the relative location estimation between two cluster leaders is also related to initial error $\|\tilde{\boldsymbol{x}}_{0_p0_q}[0]\|$, initial weight matrix $\boldsymbol{P}[0]$, forgetting factor γ, and the magnitude of the relative motion between the two rotating tags b_{pq}.*

D. Influence of Height Difference

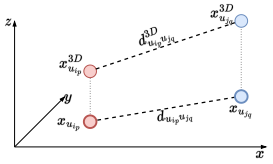

Fig. 4. The measurement distance and projection distance.

In practice, the robot tags may not be in the same horizontal plane due to the different heights being mounted. As shown in Fig. 4, $\boldsymbol{x}^{3D}_{u_{i_p}} = [x^x_{u_{i_p}}, x^y_{u_{i_p}}, x^z_{u_{i_p}}]^{\top} \in \mathbb{R}^3$ denotes the three-dimensional location of UWB tag i_p in $\mathcal{F}_w$. $d^{3D}_{u_{i_p}u_{j_q}} \in \mathbb{R}$ represents the distance of the two tags in three-dimensional

IEEE Robotics and Automation Letters (RA-L) paper, presented at ICRA 2024, Yokohama, Japan. Cite as RA-L paper.

space, which could be measured by UWB tags, while $d_{u_{i_p}u_{j_q}}$ represents the distance between the projections of the tags in the two-dimensional plane. It should be noted that $d_{u_{i_p}u_{j_q}}$ is the input of Algorithms 1 and 2 instead of $d^{3D}_{u_{i_p}u_{j_q}}$ returned by the tags. If and only if there is no height difference in the mounting positions of the tags, i.e., $x^z_{u_{i_p}} = x^z_{u_{j_q}}$, the distance measured by the tags $d^{3D}_{u_{i_p}u_{j_q}}$ is equal to the projection distance $d_{u_{i_p}u_{j_q}}$.

Theorem 3. *If the height difference between tags i_p and j_q is constant, i.e., $x^z_{u_{i_p}}[k] - x^z_{u_{j_q}}[k] = x^z_{u_{i_p}}[k-1] - x^z_{u_{j_q}}[k-1]$, then we have ${d^{3D}_{u_{i_p}u_{j_q}}}^2[k] - {d^{3D}_{u_{i_p}u_{j_q}}}^2[k-1] = d^2_{u_{i_p}u_{j_q}}[k] - d^2_{u_{i_p}u_{j_q}}[k-1]$.*

Proof. Following from the definition of the projection distance and the actual distance returned by the tags

$$d_{u_{i_p}u_{j_q}} = \sqrt{(x^x_{u_{i_p}} - x^x_{u_{j_q}})^2 + (x^y_{u_{i_p}} - x^y_{u_{j_q}})^2}, \tag{22}$$

$$d^{3D}_{u_{i_p}u_{j_q}} = \sqrt{(x^x_{u_{i_p}} - x^x_{u_{j_q}})^2 + (x^y_{u_{i_p}} - x^y_{u_{j_q}})^2 + (x^z_{u_{i_p}} - x^z_{u_{j_q}})^2}. \tag{23}$$

Thus, we have ${d^{3D}_{u_{i_p}u_{j_q}}}^2[k] - {d^{3D}_{u_{i_p}u_{j_q}}}^2[k-1] = d^2_{u_{i_p}u_{j_q}}[k] - d^2_{u_{i_p}u_{j_q}}[k-1]$, where the equation follows from the fact that the height difference between tags i_p and j_q is constant. □

Remark 7. *Theorem 3 demonstrates that if the height difference remains constant, the height difference between their UWB tags does not affect the estimation of the two-dimensional relative locations. Thus for ground mobile robots, it can be concluded that the distance $d^{3D}_{u_{i_p}u_{j_q}}$ returned by the tags can be used as the input to the Algorithms 1 and 2 to replace $d_{u_{i_p}u_{j_q}}$. For aerial robots with varying heights, their own altitude, i.e., $x^z_{u_{i_p}}$ and $x^z_{u_{j_q}}$, can be measured by ultrasonic and barometric sensors. So the inputs can be obtained by $d^2_{u_{i_p}u_{j_q}} = {d^{3D}_{u_{i_p}u_{j_q}}}^2 - (x^z_{u_{i_p}} - x^z_{u_{j_q}})^2$.*

IV. Simulation Results

A. Influence of rod length

In this simulation, both robots are stationary and not at the same height: the leader robot 0_p at $[2\,\text{m}, 3\,\text{m}, 1\,\text{m}]$ and the follower robot i_p at $[4\,\text{m}, 2\,\text{m}, 2\,\text{m}]$. In this case, although there is a height difference between the tags, the distance used in Algorithm 1 is the distance in three-dimensional space returned by the tags rather than the projection distance on the two-dimensional plane. To effectively showcase the impact of rod length l on the convergence rate, several rod lengths with significant differences have been selected for analysis, specifically $0.2\,\text{m}$, $0.35\,\text{m}$, and $0.5\,\text{m}$. In the initialization of Algorithm 1, the sampling time ΔT is set to $0.05\,\text{s}$, the forgetting factor is set to 0.999, and the initial estimation is set as $\hat{\boldsymbol{x}}_{i_p0_p}[0] = [0,0]^\top\,\text{m}$. In order to effectively demonstrate this process of convergence, the initial weight matrix has been set to a relatively diminutive value of $\boldsymbol{P}[0] = 500\boldsymbol{I}$. Moreover, generated uncorrelated uniform noise is added to the distance measurement, and the noise satisfies $U(-0.05, 0.05)\,\text{m}$.

As shown in Fig. 5, in the cases of different rod lengths, the estimation error $\tilde{\boldsymbol{x}}_{i_p0_p}$ converges to zero in the x and y dimensions. Despite the fact that the height difference exists in the z-axis, it does not affect the convergence of Algorithm 1. Thus, Theorem 3 is also verified. Moreover, as analyzed in Remark 4, the longer the rod length is, the faster the convergence rate is, and the convergence rate for $0.5\,\text{m}$ rod length is faster than the $0.35\,\text{m}$ and $0.2\,\text{m}$ cases.

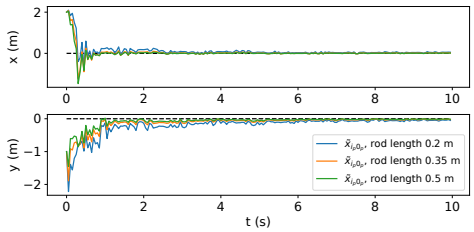

Fig. 5. Simulation results of the rotating tag with different rod lengths.

B. Influence of forgetting factor

In this simulation, five robots are considered, three belonging to cluster 1 and the other two to cluster 2. Each robot in cluster 1 has the same speed and is set to $[0.4, 2\exp(\frac{-(k-250)^2}{10000})]\,\text{m/s}$. Similarly, each robot in cluster 2 has the same speed and is set to $[0.4 + \sin(0.01\pi k), 2\exp(\frac{-(k-250)^2}{10000}) + \cos(0.02\pi k)]\,\text{m/s}$. The rod length of leader robots is assumed to be $0.25\,\text{m}$, and $0.35\,\text{m}$. The initial phases of the two rotating tags are $0\,\text{rad}$ and $\pi\,\text{rad}$, and the rotation speeds are $\pi\,\text{rad/s}$ and $2\pi\,\text{rad/s}$, respectively. The initialization of Algorithms 1 and 2 is similar to the simulation IV-A, but the generated uncorrelated uniform noise is at the $0.1\,\text{m}$ level. In order to explore the effect of forgetting factor γ on the convergence rate of the proposed algorithms in this scenario, the forgetting factor is designed as 0.97, 0.99, and 0.999, respectively. Let $E[k] = \frac{1}{4}(\|\tilde{\boldsymbol{x}}_{1_10_1}[k]\| + \|\tilde{\boldsymbol{x}}_{2_10_1}[k]\| + \|\tilde{\boldsymbol{x}}_{1_20_2}[k]\| + \|\tilde{\boldsymbol{x}}_{0_10_2}[k]\|)$.

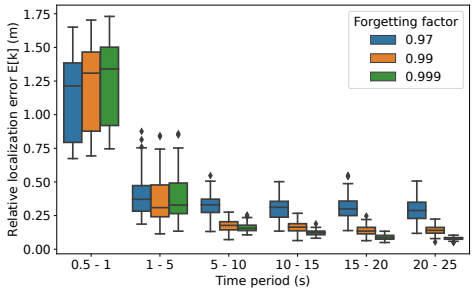

Fig. 6. The effect of forgetting factor on the convergence rate.

As shown in Fig. 6, only the results after $0.5\,\text{s}$ are shown because of the large error in the initial estimation. In the period 0.5-1 s, the larger the forgetting factor, the larger the error, while in the period 1-5 s, the forgetting factor of 0.99 has the smallest error, and in the period 5-20 s, the larger the forgetting factor, the smaller the error. Thus, it can be concluded that as the forgetting factor gradually increases, the rate of convergence also becomes slower, but the final localization accuracy improves, and the variance of the error shrinks, meaning that the resistance to noise is enhanced, confirming the analysis in Remarks 4 and 6.

IEEE Robotics and Automation Letters (RA-L) paper, presented at ICRA 2024, Yokohama, Japan. Cite as RA-L paper.

C. Influence of noise level

In this simulation, three robots with the same velocity are considered, two belonging to cluster p and one belonging to cluster q. The rod lengths and initial phase of the two rotating tags are the same as in the simulation IV-B, but the rotation speeds are -2π rad/s and 4π rad/s. For the initialization of both algorithms, $\boldsymbol{P}[0] = 10^6\boldsymbol{I}$, $\gamma = 0.9999$, and all the initial estimations are set to $[0, 0]$ m. To clearly show the localization error in different time periods, we divide the time of each simulation into three periods, T_1 represents 0-5 s, T_2 represents 5-20 s, and T_3 represents 20-40 s. In this simulation, not only the distance measurements are added with uniform noise at levels of 0.05 m, 0.1 m, and 0.2 m, respectively, but also the x and y dimensions of the velocity measurements are added with the noise of 0.05 m/s, 0.1 m/s, and 0.2 m/s, respectively.

TABLE I
RELATIVE LOCALIZATION ERRORS AT DIFFERENT NOISE LEVELS.

#		$\tilde{\boldsymbol{x}}^x_{1_p0_p}$ [m]		$\tilde{\boldsymbol{x}}^y_{1_p0_p}$ [m]		$\tilde{\boldsymbol{x}}^x_{0_p0_q}$ [m]		$\tilde{\boldsymbol{x}}^y_{0_p0_q}$ [m]	
		RMS	SD	RMS	SD	RMS	SD	RMS	SD
S_1	T_1	4.168	4.168	.5190	.4739	1.444	1.442	.5151	.5122
	T_2	.0273	.0117	.0378	.0116	.0215	.0054	.0114	.0103
	T_3	.0163	.0124	.0244	.0106	.0147	.0043	.0055	.0023
S_2	T_1	9.608	9.598	.7697	.7662	6.046	6.042	1.625	1.610
	T_2	.0794	.0361	.0325	.0272	.0232	.0230	.0184	.0113
	T_3	.0361	.0127	.0490	.0189	.0250	.0099	.0092	.0086
S_3	T_1	7.637	7.624	1.877	1.674	9.008	9.007	2.114	2.108
	T_2	.1417	.1050	.3419	.1322	.0318	.0288	.0258	.0187
	T_3	.0863	.0769	.0517	.0487	.0518	.0119	.0144	.0143

Table I shows the results, and S_1, S_2, and S_3 represent the levels of noise added to the distance and velocity as 0.05, 0.1, and 0.2, respectively. Root mean square (RMS) and standard deviation (SD) for the error in each dimension are summarized in Table I. As the noise level increases, the mean and the variance of the estimation error increases, but the error level is still significantly smaller than the noise level.

V. EXPERIMENTAL RESULTS

(a) The design of the rotating tag. (b) A screenshot of the experiments.

Fig. 7. The recording of the simulations and experiments are available at https://youtu.be/s4-UuGUBmJE.

Two mobile robots were employed to test the proposed algorithms and an overhead Vicon system was used to provide the exact absolute locations of the two robots serving as the ground truth. The velocity of each mobile robot is obtained from wheel encoders, and the distance measurements are taken from commercial UWB tags. To achieve a decentralized implementation, a ROS multi-master setup with communication over WiFi is utilized. In all the following experiments, we specify that the initial estimations are all set to $[0, 0]^\top$ m, the forgetting factors are set to 0.995, and all initial weight matrices are set to $10^6\boldsymbol{I}$.

TABLE II
THE COMPARISON OF METHODS AND ALGORITHMS.

#	$\tilde{\boldsymbol{x}}^x_{1_p0_p}$ [m]		$\tilde{\boldsymbol{x}}^y_{1_p0_p}$ [m]	
	RMS	SD	RMS	SD
Multi-tag scheme in [9]	.1861	.0981	.0736	.0710
The proposed mechanism with EKF	.2424	.1539	.2034	.1643
The proposed scheme	.1166	.0970	.0661	.0643

During the first comparison experiment, the rod length of the rotating tag was designed to be 0.1 m, and the rotation speed was set to 120 revolutions per minute (RPM). To compare the proposed algorithm with the multi-tag scheme, four tags were mounted on a circle with a radius of 0.1 m, and the algorithm described in [9] was deployed. Additionally, the extended Kalman filter (EKF) was deployed based on the data collected by the mechanics of the rotating tags. To ensure a consistent testing environment, robots 0_p and 1_p remained stationary at the same location throughout the experiments. Table II presents the results of the comparisons, which indicate that in scenarios involving small robots, the proposed localization scheme outperforms the multi-tag scheme, and the proposed algorithm is also more effective than the EKF algorithm.

The proposed algorithm is then tested in nine different scenarios, with all the rotating tags used having a rod length of 0.25 m. In the first five scenarios, Algorithm 1 for relative localization within clusters is tested, robot 0_1 is equipped with a rotating tag, while robot 1_1 has a fixed tag. During scenario E1, both robots remained stationary, whereas in scenarios E2 and E3, one of the robots moved within a 4 m $\times$ 4 m square while the other robot rotated in the center of the square. In scenarios E4 and E5, both robots moved randomly around the field through manual remote control. Furthermore, Algorithm 2 was examined between the leader robots of clusters 1 and 2 in four different scenarios, where robots 0_1 and 0_2 were each equipped with a rotating tag. In scenario E6, both robots remain stationary while one of them moves according to the square and the other rotates at the center of the square in E7. In scenarios E8 and E9, both robots move randomly. Furthermore, in these four scenarios E6-E9, robot 0_1's tag rotates clockwise at 30 RPM while robot 0_2's tag rotates counterclockwise at 30 RPM in scenarios E6 and E7, and 60 RPM in scenarios E8 and E9. As an example, the results of scenario E9 are depicted in Fig. 8.

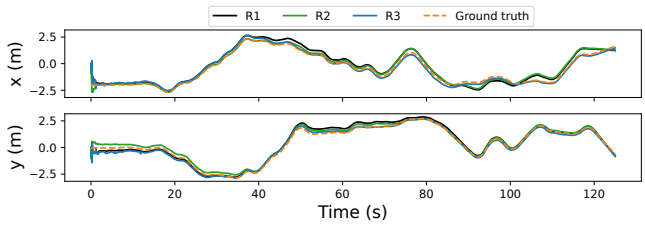

Fig. 8. Relative localization estimation and ground truth in scenario E9.

In order to avoid the effect of the initial estimation error on the estimation results, the data within five seconds from

IEEE Robotics and Automation Letters (RA-L) paper, presented at ICRA 2024, Yokohama, Japan. Cite as RA-L paper.

TABLE III
RELATIVE LOCALIZATION ESTIMATION ERROR IN DIFFERENT SCENARIOS.

#	RMS($\tilde{\boldsymbol{x}}^x_{1_1 0_1}$) [m]			SD($\tilde{\boldsymbol{x}}^x_{1_1 0_1}$) [m]			RMS($\tilde{\boldsymbol{x}}^y_{1_1 0_1}$) [m]			SD($\tilde{\boldsymbol{x}}^y_{1_1 0_1}$) [m]		
	R1	R2	R3	R1	R2	R3	R1	R2	R3	R1	R2	R3
E1	0.1330	0.0211	0.0599	0.0058	0.0016	0.0029	0.0336	0.0289	0.0145	0.0060	0.0016	0.0110
E2	0.3726	0.3034	0.1278	0.2694	0.2642	0.0265	0.3590	0.3203	0.0729	0.2783	0.2782	0.0258
E3	0.3280	0.2357	0.2074	0.2385	0.2324	0.0569	0.2517	0.2212	0.0736	0.2479	0.2004	0.0295
E4	0.2932	0.1768	0.1089	0.2741	0.1176	0.0901	0.1481	0.1255	0.0707	0.1471	0.1255	0.0498
E5	0.3552	0.2577	0.1139	0.3006	0.2407	0.0652	0.2396	0.2288	0.1623	0.2377	0.2288	0.0565
#	RMS($\tilde{\boldsymbol{x}}^x_{0_1 0_2}$) [m]			SD($\tilde{\boldsymbol{x}}^x_{0_1 0_2}$) [m]			RMS($\tilde{\boldsymbol{x}}^y_{0_1 0_2}$) [m]			SD($\tilde{\boldsymbol{x}}^y_{0_1 0_2}$) [m]		
E6	0.2485	0.0343	0.1188	0.2332	0.0064	0.0261	0.0815	0.0174	0.0668	0.0661	0.0078	0.0388
E7	0.3864	0.3511	0.0773	0.3773	0.3509	0.0703	0.3385	0.2997	0.1146	0.3380	0.2994	0.1121
E8	0.3641	0.3541	0.1007	0.3025	0.2790	0.0769	0.2601	0.2275	0.1735	0.2397	0.2268	0.1327
E9	0.3345	0.2627	0.1709	0.2737	0.2328	0.1707	0.2416	0.1960	0.1615	0.2095	0.1113	0.1473

the beginning are discarded, and the data for the next 120 seconds are recorded and summarized in Table III. The data in R1 are obtained fully based on the data returned by the on-board sensors. To clarify the effects of the noise in the distance information returned by the UWB and the noise in the velocity information returned by the wheel encoder on the estimation error, respectively, we derive the distance based on the ground truth returned by Vicon, replacing the UWB data with it, and record the estimation results in R2. Moreover, we also derive the velocity information based on Vicon, replacing the wheel encoder data, and record the results in R3. The results in Table III show that the error is around $0.3\,\mathrm{m}$, and it is worth noting that the error in scenarios E1 and E6 is significantly smaller than the other scenarios, which is due to the fact that there is almost no error in the wheel encoder when it is at stationary state. Moreover, the error of R3 in the same scenario tends to be smaller than that of R1 and R2, which indicates that velocity measurement plays an important role in estimation and the use of higher precision odometers, e.g., visual inertial odometry, helps to improve the estimation accuracy of the whole system.

VI. CONCLUSION

In this letter, a relative location estimation method based on a rotating UWB tag is proposed so that robots can estimate the relative locations of all neighbors no matter whether they are in relative motion or stationary. Our approach requires only on-board sensors as well as only one UWB tag to be installed per robot. In addition, rigorous mathematical proofs are provided, and the effects of tags height differences, rod length, and tag rotation speed on the estimation algorithms are also analyzed. Furthermore, simulations and experiments are performed to validate the proposed approach's theoretical findings and effectiveness.

REFERENCES

[1] E. Price, G. Lawless, R. Ludwig, I. Martinovic, H. H. Bülthoff, M. J. Black, and A. Ahmad, "Deep neural network-based cooperative visual tracking through multiple micro aerial vehicles," *IEEE Robotics and Automation Letters*, vol. 3, no. 4, pp. 3193–3200, 2018.

[2] B. E. Jackson, T. A. Howell, K. Shah, M. Schwager, and Z. Manchester, "Scalable cooperative transport of cable-suspended loads with uavs using distributed trajectory optimization," *IEEE Robotics and Automation Letters*, vol. 5, no. 2, pp. 3368–3374, 2020.

[3] A. Ledergerber, M. Hamer, and R. D'Andrea, "A robot self-localization system using one-way ultra-wideband communication," in *2015 IEEE/RSJ International Conference on Intelligent Robots and Systems (IROS)*. IEEE, 2015, pp. 3131–3137.

[4] K. Guo, Z. Qiu, C. Miao, A. H. Zaini, C.-L. Chen, W. Meng, and L. Xie, "Ultra-wideband-based localization for quadcopter navigation," *Unmanned Systems*, vol. 4, no. 01, pp. 23–34, 2016.

[5] W. Zhao, J. Panerati, and A. P. Schoellig, "Learning-based bias correction for time difference of arrival ultra-wideband localization of resource-constrained mobile robots," *IEEE Robotics and Automation Letters*, vol. 6, no. 2, pp. 3639–3646, 2021.

[6] Y. Wang, M. Shan, Y. Yue, and D. Wang, "Vision-based flexible leader–follower formation tracking of multiple nonholonomic mobile robots in unknown obstacle environments," *IEEE Transactions on Control Systems Technology*, vol. 28, no. 3, pp. 1025–1033, 2019.

[7] R. Liu, C. Yuen, T.-N. Do, D. Jiao, X. Liu, and U.-X. Tan, "Cooperative relative positioning of mobile users by fusing imu inertial and uwb ranging information," in *2017 IEEE International Conference on Robotics and Automation (ICRA)*. IEEE, 2017, pp. 5623–5629.

[8] B. Hepp, T. Nägeli, and O. Hilliges, "Omni-directional person tracking on a flying robot using occlusion-robust ultra-wideband signals," in *2016 IEEE/RSJ International Conference on Intelligent Robots and Systems (IROS)*. IEEE, 2016, pp. 189–194.

[9] T.-M. Nguyen, T. H. Nguyen, M. Cao, Z. Qiu, and L. Xie, "Integrated uwb-vision approach for autonomous docking of uavs in gps-denied environments," in *2019 International Conference on Robotics and Automation (ICRA)*. IEEE, 2019, pp. 9603–9609.

[10] A. Fishberg and J. P. How, "Multi-agent relative pose estimation with uwb and constrained communications," in *2022 IEEE/RSJ International Conference on Intelligent Robots and Systems (IROS)*. IEEE, 2022, pp. 778–785.

[11] S. Güler, M. Abdelkader, and J. S. Shamma, "Infrastructure-free multi-robot localization with ultrawideband sensors," in *2019 American Control Conference (ACC)*. IEEE, 2019, pp. 13–18.

[12] F.-H. O. Rajab, S. Güler, and J. S. Shamma, "Peer-to-peer localization via on-board sensing for aerial flocking," in *2020 17th International Conference on Ubiquitous Robots (UR)*. IEEE, 2020, pp. 464–471.

[13] M. Shalaby, C. C. Cossette, J. R. Forbes, and J. Le Ny, "Relative position estimation in multi-agent systems using attitude-coupled range measurements," *IEEE Robotics and Automation Letters*, vol. 6, no. 3, pp. 4955–4961, 2021.

[14] T.-M. Nguyen, Z. Qiu, T. H. Nguyen, M. Cao, and L. Xie, "Distance-based cooperative relative localization for leader-following control of mavs," *IEEE Robotics and Automation Letters*, vol. 4, no. 4, pp. 3641–3648, 2019.

[15] C. C. Cossette, M. Shalaby, D. Saussié, J. R. Forbes, and J. Le Ny, "Relative position estimation between two uwb devices with imus," *IEEE Robotics and Automation Letters*, vol. 6, no. 3, pp. 4313–4320, 2021.

[16] T.-M. Nguyen, Z. Qiu, T. H. Nguyen, M. Cao, and L. Xie, "Persistently excited adaptive relative localization and time-varying formation of robot swarms," *IEEE Transactions on Robotics*, vol. 36, no. 2, pp. 553–560, 2019.

[17] P. Batista, C. Silvestre, and P. Oliveira, "Single range aided navigation and source localization: Observability and filter design," *Systems & Control Letters*, vol. 60, no. 8, pp. 665–673, 2011.